AGU PUBLICATIONS

Geophysical Research Letters

RESEARCH LETTER
10.1002/2016GL069751

Key Points:
- Unique atmospheric, hydrologic, and geomorphic factors generated the largest flood ever recorded in the Atacama Desert
- The sediment-rich nature of the flood resulted from valley-fill erosion rather than hillslope unraveling
- Anthropogenic factors increased the consequences of the flood and highlight the need for early-warning systems

Supporting Information:
- Supporting Information S1

Correspondence to:
A. Wilcox,
andrew.wilcox@umontana.edu

Citation:
Wilcox, A. C., C. Escauriaza, R. Agredano, E. Mignot, V. Zuazo, S. Otárola, L. Castro, J. Gironás, R. Cienfuegos, and L. Mao (2016), An integrated analysis of the March 2015 Atacama floods, *Geophys. Res. Lett.*, *43*, 8035–8043, doi:10.1002/2016GL069751.

Received 26 MAY 2016
Accepted 20 JUL 2016
Accepted article online 26 JUL 2016
Published online 13 AUG 2016

An integrated analysis of the March 2015 Atacama floods

Andrew C. Wilcox[1], Cristian Escauriaza[2,3], Roberto Agredano[2,3], Emmanuel Mignot[2,4], Vicente Zuazo[2,3], Sebastián Otárola[2,3,5], Lina Castro[2,3,6], Jorge Gironás[2,3,7,8], Rodrigo Cienfuegos[2,3], and Luca Mao[9]

[1]Department of Geosciences, University of Montana, Missoula, Montana, USA, [2]Departamento de Ingeniería Hidráulica y Ambiental, Pontificia Universidad Católica de Chile, Santiago, Chile, [3]Centro de Investigación para la Gestión Integrada de Desastres Naturales (CIGIDEN), Santiago, Chile, [4]University of Lyon, INSA Lyon, CNRS, LMFA UMR5509, Villeurbanne, France, [5]Civil and Environmental Engineering and Earth Sciences, University of Notre Dame, Notre Dame, Indiana, USA, [6]Escuela de Ingeniería Civil, Pontificia Universidad Católica de Valparaíso, Valparaíso, Chile, [7]Centro de Desarrollo Urbano Sustentable (CEDEUS), Santiago, Chile, [8]Centro Interdisciplinario de Cambio Global, Pontificia Universidad Católica de Chile, Santiago, Chile, [9]Departamento de Ecosistemas y Medio Ambiente, Pontificia Universidad Católica de Chile, Santiago, Chile

Abstract In March 2015 unusual ocean and atmospheric conditions produced many years' worth of rainfall in a ~48 h period over northern Chile's Atacama Desert, one of Earth's driest regions, resulting in catastrophic flooding. Here we describe the hydrologic and geomorphic drivers of and responses to the 2015 Atacama floods. In the Salado River, we estimated a flood peak discharge of approximately 1000 m^3/s, which caused widespread damage and high sediment loads that were primarily derived from valley-fill erosion; hillslopes remained surprisingly intact despite their lack of vegetation. In the coastal city of Chañaral, flooding of the Salado River produced maximum water depths over 4.5 m, meters thick mud deposition in buildings and along city streets, and coastal erosion. The Atacama flooding has broad implications in the context of hazard reduction, erosion of contaminated legacy mine tailings, and the Atacama's status as a terrestrial analog for Mars.

1. Introduction

Large rainfall and sediment-rich flooding events struck the hyperarid Atacama Desert of northern Chile from 24 to 26 March 2015, reflecting complex interactions of the climate and the geomorphic characteristics of the region. These events were remarkable because of their human toll and their setting, in the driest area on Earth outside of Antarctica, where hillslope vegetation is largely absent and stream channels are dry or ephemeral. The March 2015 storm affected an approximately 80,000 km^2 area of the Atacama Desert. The toll of the flooding included 31 deaths, 16 people disappeared, 30,000 people displaced, and 164,000 people affected, as well as widespread damage to homes, roads, bridges, and railroads [*United Nations Office for the Coordination of Humanitarian Affairs*, 2015; *Oficina Nacional de Emergencia del Ministerio del Interior y Seguridad Pública*, 2015]. Hydrometeorological data in this remote region are sparse, hindering quantification of precipitation, discharge, and flood frequency in the basins affected by the March 2015 flooding. Infrequent, high-magnitude precipitation and flooding events have been observed in some areas of the Atacama Desert [*Houston*, 2006a], but the March 2015 event had distinctive characteristics that have never been recorded.

Understanding extreme flood events such as those documented here is important in several contexts, including reducing hazards and the human impacts of flooding, improving rainfall-runoff modeling, and understanding the role of floods in channel and landscape evolution [e.g., *Wohl*, 2000]. Here we describe the meteorological, hydrologic, and geomorphic drivers and responses to the 2015 Atacama floods. Our objectives are to characterize the forcings, water and sediment routing from source areas in the upper watershed to the outlet at the Pacific Ocean, and the urban flooding impacts of this event.

2. Study Area

The Atacama Desert extends from 18°S to 31°S and is the driest and oldest desert on Earth [*Hartley et al.*, 2005; *Amundson et al.*, 2012], with mean annual precipitation below 5 mm in its driest regions. Three factors cause aridity in the Atacama Desert: (a) the influence of the South East Pacific Anticyclone (SEPA), a subtropical

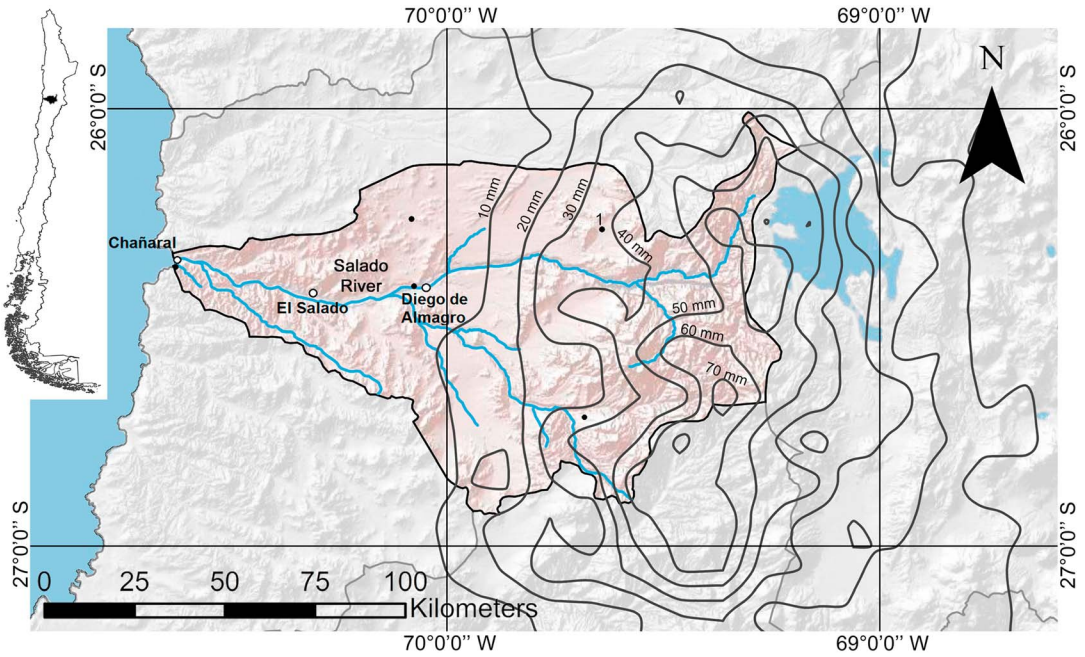

Figure 1. The Salado River basin in the Atacama Desert (inset shows location in northern Chile) and satellite-based spatial distribution of precipitation [*Huffman et al.*, 2015] during the March 2015 storm event. Precipitation was greatest over the Precordillera, in the Salado basin's headwaters, and decreased toward the basin's outlet at Chañaral on the Pacific Coast. The Andes and an endorheic basin draining to the Salar de Pedernales are to the east. Black circles denote precipitation stations used in hydrologic modeling; the Cine Inca station (denoted 1) measured hourly precipitation during the event (Figure S2a).

high-pressure system that minimizes precipitation in the region; (b) the orographic rain shadow effect of the Andes, which inhibits moisture advection from the east; and (c) the cold water upwelling to the west associated with the Pacific Ocean's Humboldt Current [*Garreaud et al.*, 2003; *Houston*, 2006a; *Jungers et al.*, 2013; *Barrett et al.*, 2016]. The onset of aridity in the Atacama has been traced to the middle Miocene; hyperarid conditions have been present for at least 2 million years [*Riquelme et al.*, 2007; *Amundson et al.*, 2012]. These climatological conditions produce an almost complete lack of vegetation in a significant portion of the Atacama Desert, which has therefore been treated as a terrestrial analog for Mars [*Navarro-González et al.*, 2003; *Stepinski and Stepinski*, 2005; *Morgan et al.*, 2014].

The March 2015 floods occurred in the southern part of the Atacama Desert and primarily influenced the Taltal, Salado, Copiapó, Huasco, and Elqui basins. Here we focus on the Salado River watershed, which received the maximum total precipitation during the event, experienced the largest river discharges, and was most severely damaged by flooding. The Salado River typically has little or no flow and is ungauged. Its basin is at approximately 26°S, in a transition zone from hyperaridity in the northern Atacama to semiaridity to the south [*Owen et al.*, 2011], and has an area of 7530 km^2 and maximum elevation of 4882 m. The basin includes zones typical of the Atacama Desert, extending from a Precordillera in the headwaters, to a Central Depression, to a Coastal Cordillera in the west. To the east and separated by a subtle topographic divide lies an endorheic basin that drains to the Salar de Pedernales [*Dorsaz et al.*, 2013], and the Andean Cordillera (Figure 1).

The Salado basin is sparsely populated, with towns built along the Salado River that largely support mines (e.g., copper mines at Potrerillos and El Salvador). The largest town is Chañaral, at the mouth of the Salado River along the Pacific Ocean (Figure 1). Coastal sediment transport typically forms a sand bar that closes the river mouth at Chañaral. Road construction on an elevated levee, composed largely of mine tailings, atop this sandbar further separated the coast from the urban area, which exacerbated flooding impacts, as described below. Deposition of an estimated $150–300 \times 10^6$ t of mine tailings within the formerly arcuate Chañaral Bay, covering an area of approximately 4 km^2 with a thickness of 10–15 m, occurred from the 1930s to 1970s and extended the coastline seaward and away from Chañaral [*Dold*, 2006]. These tailings contained copper, molybdenum sulphides, and other mining-related contaminants, resulting in elevated trace metals in the adjacent marine environment and biota [*Castilla*, 1983; *Ramirez et al.*, 2005; *Lee et al.*, 2006; *Dold*, 2006].

The drainage basin has diverse geology, characterized by lower to upper Cretaceous continental sediments and volcanic rocks, and is traversed by the north-south oriented Atacama Fault Zone [*Riquelme et al*., 2003]. Hillslopes across much of the Salado basin are mantled by Atacama Gravels, a coarse sedimentary unit hundreds of meters thick from Miocene aggradation, as a result of both aridification (reduced transport capacity) and uplift of the Coastal Cordillera [*Riquelme et al*., 2007]. Soils are thought to have formed in the last 2 million years, to be influenced by salt weathering of bedrock, and to experience transport via overland flow during extreme events [*Amundson et al*., 2012]. Very thin soils with low production rates (i.e., bedrock-to-soil conversion) and variable infiltration capacities have been documented near Chañaral, and this zone of the Atacama marks a transition from biotically to abiotically influenced hillslope processes [*Owen et al*., 2011, 2013].

The last large flood occurred on the Salado River in 1972 [*Desinventar*, 2016], but in general little is known about past flooding in the basin. Elsewhere in the Atacama, most large flooding events are associated with the South American summer monsoon, a seasonal pattern that can bring precipitation to the Atacama [*Zhou and Lau*, 1998], and with El Niño [e.g., *Magilligan et al*., 2008]. For example, large floods were documented in the Atacama Desert north of our study area in June 1991 in Antofogasta [*Ramirez and Perez*, 2011], February 2001 in the Loa River [*Houston*, 2006b], and in 2012 in the Tarapacá region [*Sepúlveda et al*., 2014].

3. Methods

In a region where few direct measurements of precipitation and discharge are available, we combine meteorological data and hydrologic and hydraulic modeling with field and aerial photograph interpretation of sediment sources and geomorphic change. The meteorology was studied from precipitation gages, the National Centers for Environmental Prediction (NCEP) 0.25 Degree Global Forecast System (GFS) historical archive, which included precipitable water output [*National Center for Atmospheric Research (NCAR)*, 2015], the NCEP/NCAR (National Center for Atmospheric Research) Reanalysis 1 data set [*National Oceanic and Atmospheric Administration (NOAA)*, 2015a], sea surface temperature (SST) data [*NOAA*, 2015b], and satellite-based Global Precipitation Measurement data [*Huffman et al*., 2015].

Because no streamflow data are available for the Salado River, we estimated the peak discharge by combining field surveys of channel geometry with a Manning equation approach. Using a differential GPS (dGPS), we surveyed channel slope, cross-section topography, and high-water marks (to determine flow depth, hydraulic radius, and flow area) after the flood event in a straight reach of the Salado River, 4 km upstream from Chañaral (supporting information Figure S1). We estimated flow resistance (and in turn velocity) by testing ranges of sediment concentration and relative bed roughness values [additional details are provided in supporting information Text S1; *Bagnold*, 1954; *Parsons et al*., 2001; *Julien*, 2010; *Takahashi*, 2014].

We also reconstructed the flood hydrograph using the U.S. Environmental Protection Agency's Storm Water Management Model (SWMM), a semidistributed rainfall-runoff model that represents a basin as a collection of subcatchments with distinct properties contributing to the channel network, through which flow is routed [*Rossman*, 2009; *Gironás et al*., 2010]. We divided the Salado basin into 11 subcatchments and assigned attributes (e.g., area and slope) to each with data from a digital elevation model. Different effective hyetographs and total effective precipitation obtained from seven stations across the watershed (Figure 1) were applied to each subcatchment. A value of the runoff coefficient C_r, which represents the ratio of runoff at the outlet to total rainfall for an event [*Chow et al*., 1988], was selected to produce a similar peak flow at Chañaral as estimated using the methods in the previous paragraph [additional details are presented in supporting information Text S2; *Reiz et al*., 1988; *Food and Agriculture Organization*, 2007].

We evaluated the geomorphic effects of the event using field observations, from the headwaters to the coastal portion of the Salado basin, completed ~1 month after the event, and aerial image analysis. To document the flood effects in Chañaral, we completed dGPS surveys and measurements of flood marks on buildings in the downtown area (supporting information Text S3). These data were combined in maps of maximum water levels. In addition, along a 85 km reach of the Salado River, extending from the mouth to ~20 km upstream of Diego de Almagro, we assessed channel change by measuring and comparing active channel width (w), defined as the width of channel with evidence of recent fluvial reworking, in preflood and postflood aerial images at 1 km intervals. Preflood and postflood channel width could not be accurately determined at all locations (e.g., because of clouds or other obstructions), so we narrowed these data to 62 locations for which we could accurately measure preflood and postflood active channel widths.

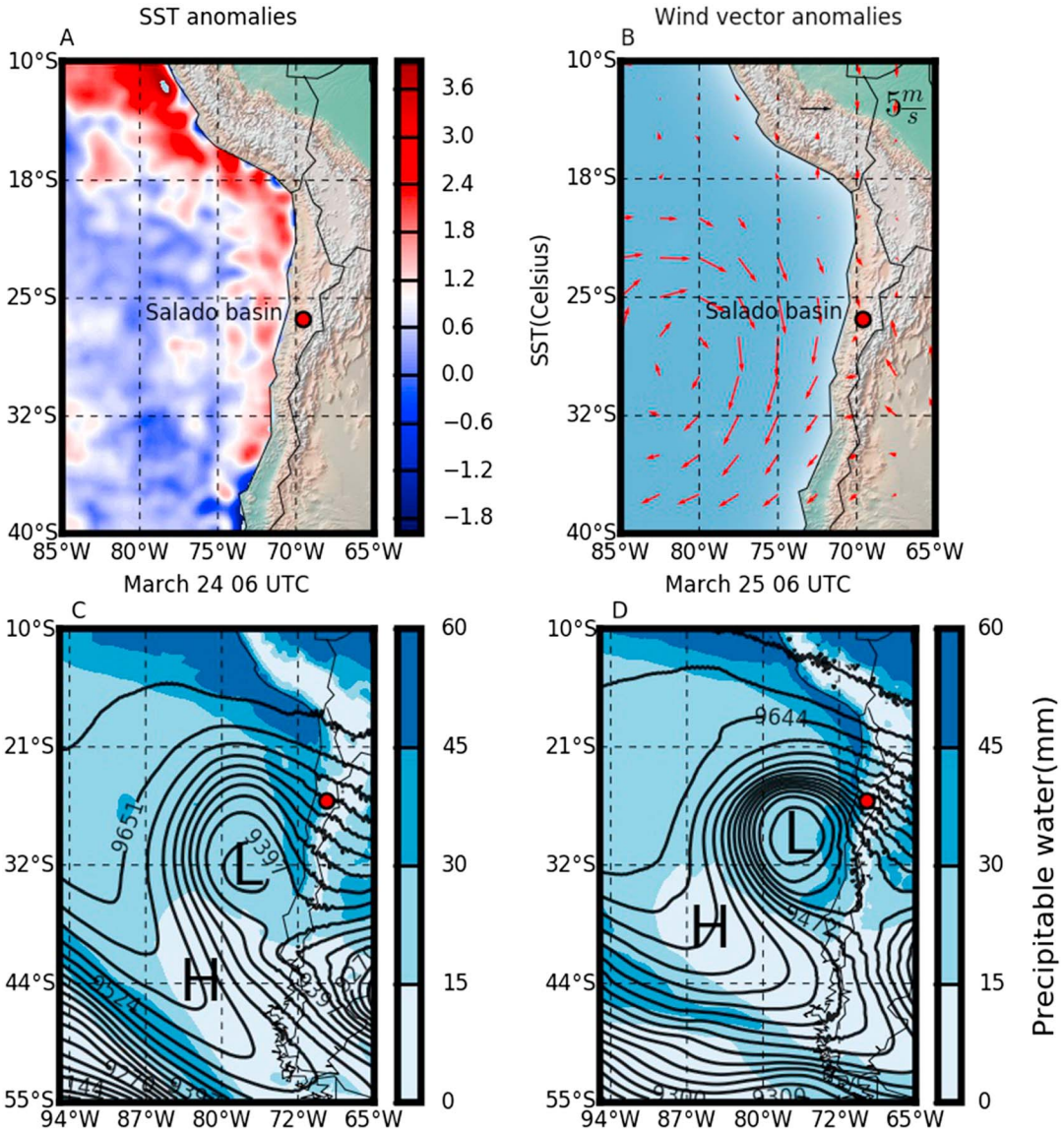

Figure 2. Oceanic and atmospheric drivers of the 2015 Atacama floods: (a) high sea surface temperature (SST) anomalies preceding the storm produced high evaporation rates and humid air that encountered the low-pressure zone shown in Figures 2c and 2d; (b) wind speed anomalies during the dates of the events (the historical mean has been subtracted) are cyclonic (clockwise), contrary to the South East Pacific Anticyclone typically present in this region; (c and d) geopotential height contours at 300 hPa (black lines) overlain on precipitable water (colored contours), illustrating that a cutoff low-pressure system (denoted L) built off the coast and reached inland on 24 March 2015 and strengthened by 25 March, accompanied by high amounts of precipitable water coming from the north.

4. Results

4.1. Atmospheric and Oceanic Drivers and Resulting Precipitation

A confluence of unusual oceanic and atmospheric conditions set the stage for the March 2015 Atacama floods. Very high SST anomalies off the coast of northern Chile, up to +3°C (Figure 2a), may have reflected warming of the eastern equatorial Pacific Ocean during the 2015 El Niño [*Bell et al.*, 2015; *Barrett et al.*, 2016]. Moreover, the NCEP/NCAR GFS and reanalysis data suggest weakening of the SEPA at this time; cyclonic (clockwise) patterns of wind-velocity fluctuations at 1000 hPa from 22 to 28 March (Figure 2b) illustrate a reversal of the normal anticyclone conditions. As a result a low-pressure system built off the coast of Chile and moved inland starting on 24 March (Figure 2c) and strengthening on 25 March (Figure 2d), when the greatest precipitation occurred over the study area. A core of cold air in the middle and upper troposphere trapped moist air moving inland over the warmer-than-normal ocean, producing a cutoff low (COL) pressure system [*Fuenzalida et al.*, 2005; *Garreaud and Fuenzalida*, 2007]. The warm ocean conditions would have also

contributed to attenuation of the SEPA, promoted evaporation, and contributed to high amounts of precipitable water (Figures 2c and 2d) along the northern Chile coastline. The combination of anomalously high amounts of precipitable water and an unstable atmosphere, due to the presence of the COL, produced inland flow of warm, moist air and record rainfall over the upper Salado basin and its environs [*Barrett et al*., 2016].

The greatest amount of precipitation fell in the upper Salado basin, over the Precordillera. All precipitation occurred as rain rather than snow, including at elevations exceeding 4000 m in the headwaters, reflecting the warm nature of the storm. Precipitation data from a rain gage northeast of Diego de Almagro (Cine Inca, 2240 m elevation; Figure 1) show multiple (at least three) pulses of precipitation over a 51 h period, with maximum rates of 7.5 mm/h and total rainfall of 77 mm (Figure S2a). Similar magnitudes were recorded at other nearby rain gages at similar elevation, including 80 mm from a gage southeast of Diego de Almagro (elevation 2,250 m) and 87 mm from a gage at El Salvador, just outside of the Salado basin and northeast of Diego de Almagro [*Barrett et al*., 2016]. In coastal areas, where flood damages were greatest, precipitation was much lower; gages at Chañaral recorded total precipitation of ~20 mm [*Olea and Arce*, 2015]. Satellite data [*Huffman et al*., 2015] showed strong orographic gradients of precipitation (Figure 1), with estimated totals over the Precordillera in the range of 50–70 mm. Comparison to data from gages in those locations suggests that the satellite-based precipitation totals were underestimates.

4.2. Hydraulic and Hydrologic Reconstruction and Urban Impacts

We estimated peak discharges of 1450 m^3/s (water-sediment mixture) and 1150 m^3/s (water only) at the entrance of Chañaral. These values are averages over a range of sediment concentration and relative bed roughness values (Figure S3); the coefficient of variation of discharge estimates was 0.16. At the only gage in the region that measured discharge during the event, in upper reaches of the adjacent Copiapó River basin, the peak flow was 36 m^3/s [Copiapó en Pastillo station, elevation 1305 m; Figure S2b; *DICTUC*, 2010].

Modeling using SWMM provides an alternative approach to reconstructing flood hydrology. A calibrated value of $C_r = 0.06$ in SWMM produced a peak, clear-water discharge of ~1000 m^3/s at Chañaral, as well as peak discharges of 310 and 800 m^3/s for the towns of Diego de Almagro and El Salado, respectively (Figure S4). Modeled peak discharge estimates are highly sensitive to C_r (Figure S4). For comparison to the C_r value used in SWMM, we deduced a value of $C_r = 0.02$ in the adjacent Copiapó River basin from the volumetric record in a local reservoir and the upstream contributing precipitation. Both C_r values are within the range reported for extremely arid regions [*Kidron and Pick*, 2000; *Cantón et al*., 2001; *Yair and Raz-Yassif*, 2004] and indicate low rates of overland flow on hillslopes (see Text S2 for additional discussion of C_r values).

In the urban area of Chañaral, high-water and mud markings on roads and infrastructure showed that the town experienced zones of both high flow velocity, reaching approximately 8 m/s (estimated from the Manning equation and measured high-water marks), and dammed, low-velocity flow (Figure 3). Flooding in Chañaral occurred in two distinct phases. First, culverts that normally passed Salado River flow beneath Highway 5, which was built on an elevated levee constructed using legacy mining sediments (3 m above the lower parts of the city), were overwhelmed and blocked, damming flow southeast of the highway and causing flow stagnation, inundation, and massive mud deposition in buildings and on the streets of low-elevation portions of Chañaral. Maximum water depths of 2.5–2.7 m were documented, with decreasing depths with distance southeast from the highway (Figure 3 and Text S3). Horizontal flood marks on buildings in the downtown area of Chañaral, which were similar inside and outside the buildings, provided evidence of very low flow velocities during this period (Figures S6–S8). Second, as the water level increased in Chañaral as a result of the damming effect of the highway, eventually water overtopped the highway and produced two significant breaches. One breach was more than 450 m wide and in the vicinity of the Salado River channel; this breach allowed high-velocity river flow directly toward the Pacific Ocean, resulting in scouring of buildings and other dramatic damage in the areas bordering the channel. A second breach, to the south, was about 300 m wide, permitted evacuation of water from the downtown area and produced erosion at the outlet of the breach (Figure 3). Additional mud deposition likely occurred as floodwaters receded, but our observations suggest that the greatest deposition occurred earlier during the event.

4.3. Flood Geomorphology: Sediment Sources and Geomorphic Change

A remarkable element of the flood, particularly with respect to its effects on urban areas, was its high sediment load. No measurements of fluxes or concentrations are available, but observations of videos from the

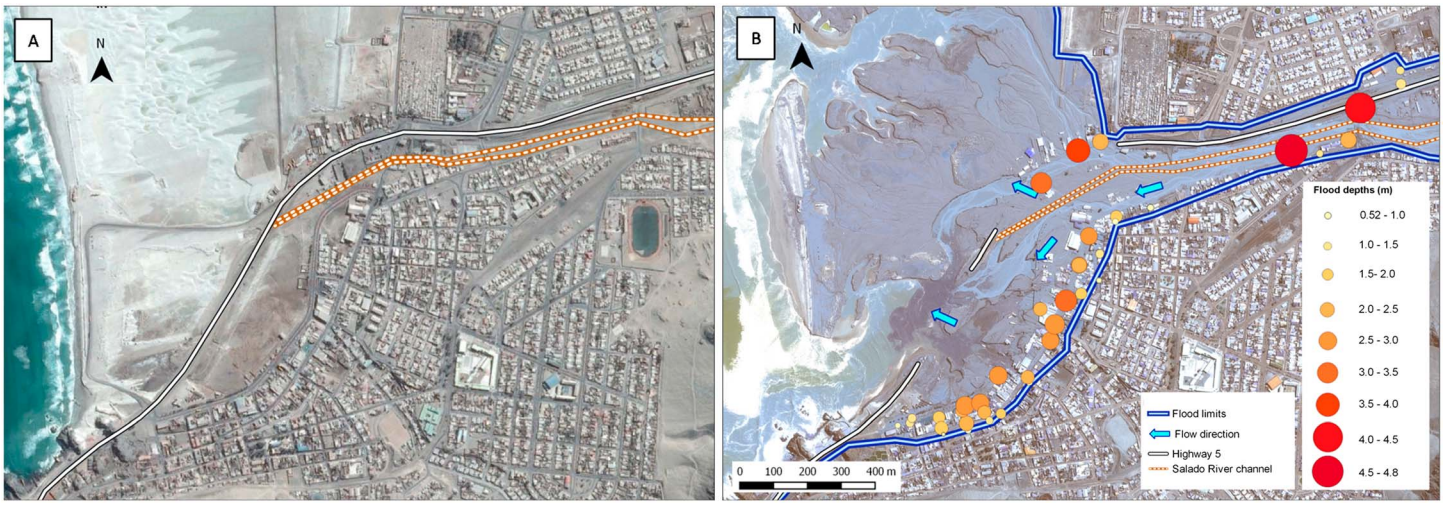

Figure 3. Chañaral at the Salado River mouth: (a) preflood image (22 July 2013) showing coastline location, Highway 5 and channelized Salado River; (b) postflood image (27 March 2015) showing coastal erosion and breaches of Highway 5, measured flow depths, estimated flow direction, and flood limits (Google Earth, Fuerza Aérea de Chile).

flood event and of postflood mud deposits indicate that suspended sediment concentrations were high enough to produce hyperconcentrated flow.

Observations in the upper watershed, where the greatest precipitation occurred, indicated widespread rilling and gullying initiated by overland flow (Figure S9). Rills or gullies did not show evidence of progressive bulking (i.e., enlargement and entrainment of additional sediment in a downslope direction); however, rills were typically shallow, linear features showing no consistent spacing or clear initiation threshold. Moreover, sediment from these sources typically did not reach valley bottoms; rills and gullies typically faded near the base of the hillslopes (i.e., at the footslope), with small, individual fan-like sediment deposits debouching from each feature on footslopes. Moreover, we observed only limited, small-scale mass wasting during field surveys, typically as shallow translational slides (Figure S8) or rockfall where hillslopes had been undercut by channel erosion; the overall contribution to fluvial sediment flux from mass movements appeared to have been negligible.

Whereas hillslope sediment delivery to channels was surprisingly small, dramatic erosion of valley fills occurred. Field observations indicated that the sediment load was primarily derived from erosion of channel bed, bank, and floodplain material (i.e., valley fill). Aerial photograph analysis found that the scaled change in active channel width $[(w_{post} - w_{pre})/w_{pre}]$ was 2.3 ± 8.6; i.e., on average, active channel width more than doubled, with large variation (Figures S10–S12). No channel-widening trend was observed in the downstream direction. Although widening was the primary erosion mechanism and sediment source, channel incision was also evident along many reaches, especially in valleys confined by either hillslopes or by infrastructure (roads and railroads).

Flooding also altered the morphology of the mouth of the Salado River and produced dramatic coastal erosion, likely following the highway breach described above. In places the shoreline receded by 500–1000 m (Figures S3, S8, and S13). Much of the eroded coastal material consisted of mine tailings that had previously deposited in Chañaral Bay.

5. Discussion and Conclusions

The 2015 Atacama floods resulted from a confluence of unusual ocean and atmospheric conditions that produced a cutoff low-pressure system that moved inland, high amounts of precipitable water, and warm, intense storms concentrated over the upper Salado basin. Meteorologic conditions, COL development, and the anomalously high precipitable water driving this event are also described by *Barrett et al.* [2016], who also document extreme warm temperatures in central and southern Chile preceding and concurrent with the March 2015 floods. Dynamics of COL systems such as the one implicated here, and of their interactions with

the Andes, have also been simulated using the Weather Research and Forecasting model by *Garreaud and Fuenzalida* [2007]. They showed that the Andes influences COL systems by, on the one hand, obstructing the inflow of warm, moist air from the interior that would otherwise cause convection and COL weakening and, on the other hand, contributing to COL dissipation as a result of latent heat release associated with cloud formation over the Andes [*Fuenzalida et al*., 2005; *Garreaud and Fuenzalida*, 2007].

Accurate measures of peak flow magnitude are typically lacking for large floods in the Atacama Desert, but comparison to published reports [e.g., *Houston*, 2006b] suggests that the March 2015 event was the heaviest and most extensive *documented* rainfall, producing the largest *documented* floods, in the region. For example, flood magnitudes measured in the adjacent Copiapó River were by far the largest since gaging began in 1971 (the previous peak discharge at the Copiapó en Pastillo station was ~23 m^3/s, compared to 36 m^3/s in March 2015). The only documented large flood in the Salado River, in February 1972, was smaller than the March 2015 event, judging from ground photographs of Chañaral taken after the event; to the best of our knowledge, its peak flow was neither measured nor estimated.

The floods were unusual not only in their magnitude but also in terms of their high sediment supply, which produced high-sediment-concentration flows and extensive mud deposition in urban areas. Previous work has suggested that during extreme precipitation and flooding events in the Atacama, landslides and debris flows are widespread and an important sediment source, as would be expected in areas with low infiltration capacity and hillslopes dissected by ravines [*Sepúlveda et al*., 2014]. The erosional response we observed differed from this; however, field observations indicated that hillslope erosion was largely restricted to rilling rather than debris flows and that interrill erosion was limited and hillslopes were largely stable. These observations were consistent with both the calibrated value of C_r used in our rainfall-runoff modeling, and with *Owen et al.*'s [2013] finding of spatially variable infiltration rates near Chañaral. Rilling observed on hillslopes provided evidence of low infiltration capacities, whereas limited interrill erosion and the tendency of rills to dissipate rather than growing into gullies or debris flows suggested locally higher infiltration rates (e.g., along footslopes), although spatial variability in infiltration rates likely lessened as the storm progressed [e.g., *Yair and Raz-Yassif*, 2004] and runoff rates to valley bottoms increased. Although vegetation is absent on hillslopes, the absence of hillslope unraveling suggests that soil characteristics (e.g., the Atacama Gravels, desert pavement, and salt crusts [*Riquelme et al*., 2007; *Davis et al*., 2010; *Owen et al*., 2013]) may have produced cohesion and stabilized slopes. Regardless, the magnitude of flooding, and our field observations, provide clear evidence that the March 2015 event generated runoff to valley bottoms with sufficient stream power to produce widespread lateral and vertical erosion of valley fill that comprised most of the flood's sediment supply.

Flood damages were a consequence of the high-magnitude discharge and sediment-rich nature of the flood and also were exacerbated by land uses and infrastructure. In the upper watershed, roads and railroads confined the channel in many locations, concentrating flood energy and increasing incision and valley-fill erosion. Building construction immediately adjacent to the channel (e.g., in Diego de Almagro) created flow resistance, promoted sediment deposition, resulted in extensive damages, and illustrated low awareness of flood potential. In Chañaral, road infrastructure and obstructed culverts reduced channel capacity and blocked the flood's path to Chañaral Bay, damming the flow and greatly increasing flood extent, mud deposition, and associated damages, after which breaching of the highway produced rapid channel flow, erosion, and building removal. Overall patterns of erosion and deposition therefore reflected not only downstream increases and decreases in stream power, as documented for other extreme floods [*Gartner et al*., 2015], but also local infrastructure effects. Headward erosion of contaminated mine tailings along the coast may have also produced contamination of the adjacent marine environment, as has previously been documented in Chañaral Bay [*Ramirez et al*., 2005], highlighting the long-term challenges of managing mining-contaminated sediments.

Meteorologists predicted unusual atmospheric conditions and high-magnitude precipitation in advance of this event [*Centro de Ciencia del Clima y la Resiliencia*, 2015], but those predictions were not translated into flood predictions to encourage flood preparation or evacuations [*El Mostrador*, 2015], highlighting key gaps between science and management. The 2015 Atacama floods reinforce *Rasmussen et al.*'s [2014] call for improved understanding of weather events in South America in order to reduce the death and economic tolls of extreme events such as floods. The floods also point to the need to reduce flood fatalities by discouraging human settlement in flood-prone areas and by taking better advantage of Earth observation data to improve early-warning systems, planning for extreme events, and disaster response [*Pappenberger et al*., 2008; *Di Baldassarre et al*., 2010; *Schumann et al*., 2016].

Acknowledgments

This research was funded by Conicyt/Fondap grant 15110017. C.E. was supported by Fondecyt grant 1130940. J.G. also acknowledges Conicyt/Fondap grant 15110020. ACW was supported by a Fulbright Visiting Scholars grant. E.M. was supported by a scholarship from the School of Engineering of PUC University (Chile). We thank Kurt Imhoff for assistance with aerial photo analysis. We also thank Ron Amundson and Enrique Vivoni for comments that improved the manuscript and Servicio Aerofotogramétrico de la Fuerza Aérea de Chile (SAF) for satellite imagery. The data used here are available on request from the first author.

References

Amundson, R., et al. (2012), Geomorphologic evidence for the late Pliocene onset of hyperaridity in the Atacama Desert, *Geol. Soc. Am. Bull.*, *124*, 1048–1070.

Bagnold, R. A. (1954), Experiments on a gravity-free dispersion of large solid spheres in a Newtonian fluid under shear, *Proc. R. Soc. London A*, *225*(1160), 49–63.

Barrett, B. S., D. A. Campos, J. Vicencio Veloso, and R. Rondanelli (2016), Extreme temperature and precipitation events in March 2015 in central and northern Chile, *J. Geophys. Res. Atmos.*, *121*, 4563–4580, doi:10.1002/2016JD024835.

Bell, G. D., W. Shi, M. L'Heureux, and M. Halpert (2015), *Climate Diagnostics Bulletin*, NOAA/NWS/NCEP Clim. Predict. Cent, College Park, Maryland. [Available at http://www.cpc.ncep.noaa.gov/products/CDB/CDB_Archive_html/bulletin_032015/, accessed 23 June 2016.]

Cantón, Y., F. Domingo, A. Solé-Benet, and J. Puigdefábregas (2001), Hydrological and erosion response of a badlands system in semiarid SE Spain, *J. Hydrol.*, *252*(1), 65–84.

Castilla, J. C. (1983), Environmental impact in sandy beaches of copper mine tailings at Chañaral, Chile, *Mar. Pollut. Bull.*, *14*, 459–464.

Chow, V. T., D. Maidment, and L. W. Mays (1988), *Applied Hydrology*, McGraw Hill, New York.

Centro de Ciencia del Clima y la Resiliencia (2015), "Norte oscuro, sur claro," por René Garreaud, Centro de Ciencia del Clima y la Resiliencia (CR2), 26 March. [Available at http://www.cr2.cl/norte-oscuro-sur-claro/, accessed 30 June 2016.]

Davis, W. L., I. de Pater, and C. P. McKay (2010), Rain infiltration and crust formation in the extreme arid zone of the Atacama Desert, Chile, *Planet. Space Sci.*, *58*(4), 616–622.

Desinventar (2016), Inventory system of the effects of disasters. [Available at http://www.desinventar.org/, accessed 25 March 2016.]

Di Baldassarre, G., A. Montanari, H. Lins, D. Koutsoyiannis, L. Brandimarte, and G. Blöschl (2010), Flood fatalities in Africa: From diagnosis to mitigation, *Geophys. Res. Lett.*, *37*, L22402, doi:10.1029/2010GL045467.

DICTUC (2010), Análisis Integrado de Gestión en Cuenca del Río Copiapó, *Rep. 901825*, prepared by DICTUC. Pontificia Univ. Católica de Chile for the Minist. of Public Works. [Available at http://documentos.dga.cl/ADM5220v1.pdf.]

Dold, B. (2006), Element flows associated with marine shore mine tailings deposits, *Environ. Sci. Technol.*, *40*, 752–758.

Dorsaz, J. M., J. Gironás, C. Escauriaza, and A. Rinaldo (2013), The geomorphometry of endorheic drainage basins: Implications for interpreting and modelling their evolution, *Earth Surf. Processes Landforms*, *38*, 1881–1896.

El Mostrador (2015), Meteorología asegura que la Onemi estaba informada antes del riesgo por las lluvias en Atacama, 26 March. [Available at http://www.elmostrador.cl/destacado/2015/03/26/meteorologia-asegura-que-la-onemi-estaba-informada-antes-del-riesgo-por-las-lluvias-en-atacama/, accessed 30 June 2016.]

Food and Agriculture Organization (2007), Digital soil map of the world. version 3.6. [Available at http://www.fao.org/geonetwork/srv/en/metadata.show?id=14116.]

Fuenzalida, H., R. Sanchez, and R. Garreaud (2005), A climatology of cutoff lows in the Southern Hemisphere, *J. Geophys. Res.*, *110*, D18101, doi:10.1029/2005JD005934.

Garreaud, R., and H. Fuenzalida (2007), The influence of Andes on cutoff lows: A modeling study, *Mon. Weather Rev.*, *135*, 1596–1613.

Garreaud, R., M. Vuille, and A. C. Clement (2003), The climate of the Altiplano: Observed current conditions and mechanisms of past changes, *Palaeogeogr. Palaeoclimatol. Palaeoecol.*, *194*(1), 5–22.

Gartner, J. D., W. B. Dade, C. E. Renshaw, F. J. Magilligan, and E. M. Buraas (2015), Gradients in stream power influence lateral and downstream sediment flux in floods, *Geology*, *43*(11), 983–986.

Gironás, J., L. A. Roesner, L. A. Rossman, and J. Davis (2010), A new applications manual for the Storm Water Management Model (SWMM), *Environ. Modell. Software*, *25*(6), 813–814.

Hartley, A. J., G. Chong, J. Houston, and A. E. Mather (2005), 150 million years of climatic stability: Evidence from the Atacama Desert, northern Chile, *J. Geol. Soc.*, *162*, 421–424.

Houston, J. (2006a), Variability of precipitation in the Atacama Desert: Its causes and hydrological impact, *Int. J. Climatol.*, *26*, 2181–2198.

Houston, J. (2006b), The great Atacama flood of 2001 and implications for Andean hydrology, *Hydrol. Processes*, *20*, 591–610.

Huffman, G., D. T. Bolvin, and E. J. Nelkin (2015), Integrated Multi-satellitE Retrievals for GPM (IMERG) technical documentation, NASA Goddard Space Flight Center, 19 June. [Available at http://pmm.nasa.gov/sites/default/files/document_files/IMERG_doc.pdf.]

Julien, P. (2010), *Erosion and Sedimentation*, Cambridge Univ. Press, Cambridge, U. K.

Jungers, M. C., A. M. Heimsath, R. Amundson, G. Balco, D. Shuster, and G. Chong (2013), Active erosion-deposition cycles in the hyperarid Atacama Desert of Northern Chile, *Earth Planet. Sci. Lett.*, *371–372*, 125–133.

Kidron, G. J., and K. Pick (2000), The limited role of localized convective storms in runoff production in the western Negev Desert, *J. Hydrol.*, *229*(3), 281–289.

Lee, M. R., J. A. Correa, and R. Seed (2006), A sediment quality triad assessment of the impact of copper mine tailings disposal on the littoral sedimentary environment in the Atacama region of northern Chile, *Mar. Pollut. Bull.*, *52*, 1389–1395.

Magilligan, F., P. S. Goldstein, G. Fisher, B. Bostick, and R. Manners (2008), Late Quaternary hydroclimatology of a hyper-arid Andean watershed: Climate change, floods, and hydrologic responses to the El Niño-Southern Oscillation in the Atacama Desert, *Geomorphology*, *101*(1), 14–32.

Morgan, A. M., A. D. Howard, D. E. Hobley, J. M. Moore, W. E. Dietrich, R. M. E. Williams, D. M. Burr, J. A. Grant, S. A. Wilson, and Y. Matsubara (2014), Sedimentology and climatic environment of alluvial fans in the Martian Saheki crater and a comparison with terrestrial fans in the Atacama Desert, *Icarus*, *229*, 131–156.

National Center for Atmospheric Research (2015), NCEP GFS 0.25 Degree global forecast auxiliary grids historical archive, Res. Data Arch. at the Natl. Cent. for Atmos. Res., Comput. & Inf. Syst. Lab. [Available at http://rda.ucar.edu/datasets/ds084.3/.]

National Oceanic and Atmospheric Administration (NOAA) (2015a), National Center for Environmental Prediction/National Center for Atmospheric Research (NCEP/NCAR) reanalysis summary, Earth Syst. Res. Lab. Phys. Sci. Div. [Available at http://www.esrl.noaa.gov/psd/data/gridded/data.ncep.reanalysis.html.]

National Oceanic and Atmospheric Administration (NOAA) (2015b), Sea surface temperature (SST) high-resolution dataset, Earth Syst. Res. Lab. Phys. Sci. Div. [Available at http://www.esrl.noaa.gov/psd/data/gridded/data.noaa.oisst.v2.highres.html.]

Navarro-González, R., et al. (2003), Mars-like soils in the Atacama Desert, Chile, and the dry limit of microbial life, *Science*, *302*(5647), 1018–1021.

Oficina Nacional de Emergencia del Ministerio del Interior y Seguridad Pública (2015), Monitoreo por evento hidrometeorológico, 7 June. [Available at http://www.onemi.cl/alerta/monitoreo-por-evento-hidrometeorologico/, accessed 30 June 2016.]

Olea, P., and S. Arce (2015), Caracterización de las principales cuencas afectadas durante el evento meteorológico del 24 y 26 de Marzo de 2015, *Rep. INF-HIDROLOGIA-01*, prepared for Sernageomin, Minist. of Min., 29 May.

Owen, J. J., R. Amundson, W. E. Dietrich, K. Nishiizumi, B. Sutter, and G. Chong (2011), The sensitivity of hillslope bedrock erosion to precipitation, *Earth Surf. Processes Landforms*, *36*(1), 117–135, doi:10.1002/esp.2083.

Owen, J. J., W. E. Dietrich, K. Nishiizumi, G. Chong, and R. Amundson (2013), Zebra stripes in the Atacama Desert: Fossil evidence of overland flow, *Geomorphology*, *182*, 157–172.

Pappenberger, F., J. Bartholmes, J. Thielen, H. L. Cloke, R. Buizza, and A. de Roo (2008), New dimensions in early flood warning across the globe using grand-ensemble weather predictions, *Geophys. Res. Lett.*, *35*, L10404, doi:10.1029/2008GL033837.

Parsons, J. D., K. X. Whipple, and A. Simioni (2001), Experimental study of the grain-flow, fluid-mud transition in debris flows, *J. Geol.*, *109*, 427–447.

Ramirez, F. J., and P. C. Perez (2011), Passing volume calculation system (PVCS): Computer software for managing data on watersheds that produce mud flows and the case of Quebrada La Cadena, Antofagasta, Chile, *Nat. Hazards*, *59*(1), 149–166, doi:10.1007/s11069-011-9744-5.

Ramirez, M., S. Massolo, R. Frache, and J. A. Correa (2005), Metal speciation and environmental impact on sandy beaches due to El Salvador copper mine, Chile, *Mar. Pollut. Bull.*, *50*(1), 62–72.

Rasmussen, K. L., M. D. Zuluaga, and R. A. Houze Jr. (2014), Severe convection and lightning in subtropical South America, *Geophys. Res. Lett.*, *41*, 7359–7366, doi:10.1002/2014GL061767.

Reiz, C., P. Maulder, and L. Begemann (1988), *Water Harvesting for Plant Production*, *Tech. Pap. 91*, World Bank, Washington, D. C.

Riquelme, R., J. Martinod, G. Herail, J. Darrozes, and R. Charrier (2003), A geomorphological approach to determining the Neogene to recent tectonic deformation in the Coastal Cordillera of northern Chile (Atacama), *Tectonophysics*, *361*, 255–275.

Riquelme, R., G. Hérail, J. Martinod, R. Charrier, and J. Darrozes (2007), Late Cenozoic geomorphologic signal of Andean forearc deformation and tilting associated with the uplift and climate changes of the Southern Atacama Desert (26°S–28°S), *Geomorphology*, *86*, 283–306.

Rossman, L. (2009), *Storm Water Management Model User's Manual Version 5.0*, *EPA/600/R-05/040*, U.S. Environ. Prot. Agency, Water Supply and Water Resour. Div., Natl. Risk Manage. Res. Lab., Cincinnati, Ohio.

Schumann, G. J. P., et al. (2016), Unlocking the full potential of Earth observation during the 2015 Texas flood disaster, *Water Resour. Res.*, *52*, 3288–3293, doi:10.1002/2015WR018428.

Sepúlveda, S. A., S. Rebolledo, J. McPhee, M. Lara, M. Cartes, E. Rubio, D. Silva, N. Correia, and J. P. Vásquez (2014), Catastrophic, rainfall-induced debris flows in Andean villages of Tarapacá, Atacama Desert, northern Chile, *Landslides*, *11*, 481–491.

Stepinski, T., and A. Stepinski (2005), Morphology of drainage basins as an indicator of climate on early Mars, *J. Geophys. Res.*, *110*, E12S12, doi:10.1029/2005JE002448.

Takahashi, T. (2014), *Debris Flows: Mechanics, Prediction and Countermeasures*, 2nd ed., CRC Press/Balkema, Leiden, Netherlands.

United Nations Office for the Coordination of Humanitarian Affairs (2015), Chile: Floods and mudslides, 3 pp., 14 April. [Available at http://reliefweb.int/report/chile/chile-floods-and-mudslides-informative-note-14-april-2015.

Wohl, E. E. (2000), *Inland Flood Hazards: Human, Riparian, and Aquatic Communities*, Cambridge Univ. Press, Cambridge.

Yair, A., and N. Raz-Yassif (2004), Hydrological processes in a small arid catchment: Scale effects of rainfall and slope length, *Geomorphology*, *61*(1), 155–169.

Zhou, J., and K.-M. Lau (1998), Does a monsoon climate exist over South America?, *J. Clim.*, *11*, 1020–1040.